Computers in Biology and Medicine 104 (2019) 87–96

Contents lists available at ScienceDirect

Computers in Biology and Medicine

journal homepage: www.elsevier.com/locate/compbiomed

Periodically kicked network of RLC oscillators to produce ECG signals

M.A. Quiroz-Juárez [a], O. Jiménez-Ramírez [b], J.L. Aragón [a], J.L. Del Río-Correa [c], R. Vázquez-Medina [d,*]

[a] Centro de Física Aplicada y Tecnología Avanzada, Universidad Nacional Autónoma de México, Boulevard Juriquilla 3001, Juriquilla, 76230, Querétaro, Mexico
[b] Instituto Politécnico Nacional, Escuela Superior de Ingeniería Mecánica y Eléctrica, Unidad Culhuacán. Santa Ana 1000, San Francisco Culhuacán, 04430, Ciudad de México, Mexico
[c] Departamento de Física, Universidad Autónoma Metropolitana, Unidad Iztapalapa, San Rafael Atlixco 186, 09340, Iztapalapa, Ciudad de México, Mexico
[d] Instituto Politécnico Nacional, Centro de Investigación en Ciencia Aplicada y Tecnología Avanzada, Cerro Blanco 141, Colinas del Cimatario, 76090, Querétaro, Mexico

ARTICLE INFO

Keywords:
ECG signals
Heart model
RLC circuit
Periodically-kicked oscillators

ABSTRACT

We propose a simple model of the electrical activity of the heart that reproduces realistic healthy electrocardiogram (*ECG*) signals. The model consists of two *RLC* linear oscillators periodically kicked by impulses of the main pacemaker with the frequency rate of a real heart. In the proposed model, one oscillator represents the atria, another represents the ventricles, and an electrical cardiac conduction system is included using a coupling capacitor, which can be either unidirectional or bidirectional. The network of the two capacitively coupled oscillators is periodically kicked by the main pacemaker to introduce the periodic forcing of limit cycles into the system; a time delay is introduced to represent the electrical transport delay from atria to ventricles. In this manner, healthy synthetic *ECG* signals are obtained by combining the signals of the currents of the oscillators. We show that an analytical solution of the model can be obtained when a single impulse is applied. From this, by the superposition principle, a solution with an impulse train is obtained. Note that analytical treatment is a feature not available in current cardiac oscillator models.

1. Introduction

The heart is one of the most studied organs of the body, and many studies aim to understand the roots of either mechanical or electrical failures [1–3]. Electrical signals, governed by activation potentials controlled by a group of specialized cells, coordinate the mechanical activity of the heart. This process occurs as follows. Action potentials originate in the sinoatrial (*SA*) node, located in the right atrium at the superior vena cava. The electrical pulse propagates through the atrium, which produces a contraction. The atrioventricular (*AV*) node lies in the wall of tissue between the atria and ventricles and delays electrical activation to allow the contraction and the filling of atrial and ventricular cavities with blood.

The pulse propagation from the *AV* node to the ventricles is provide by a specialized conduction system called the His-Purkinje complex (*HP*), which conducts the electrical impulse to produce the coordinated contraction of the ventricles, resulting in the effective pumping of blood to the body [4] (Ch. 12). In the cardiac tissue, a process of recovery (repolarization) initiates after each electrical excitation (depolarization) to prepare it for the next electrical stimulation.

A normal cardiac electrical cycle ranges from 60 to 80 beats per minute and electrocardiograms (*ECGs*) at different points on the surface of the body can monitor it noninvasively. A single normal cycle of the *ECG* signals represents the successive processes of atrial depolarization/repolarization and ventricular depolarization/repolarization, which occur with every heartbeat [5]. These processes can be related to the peaks and troughs of the *ECG* waveform, labeled *P Q*, *R*, *S* and *T*. The *P* wave is linked with the excitation of the atria, the *QRS* complex with excitation of the ventricles, and the *T* wave with recovery of the excitability of ventricles.

The development of dynamical models to produce *ECG* signals has been the subject of many research efforts [6–8]. Several mathematical models to produce synthetic *ECG* signals have been developed [9–11], all of them based on nonlinear equations, thus making the analytical treatment often prohibitive and requiring numerical tools.

Some of the proposed models are based on a dynamical system on a circle. McSharry et al. [12], for example, proposed a dynamical model based on three coupled ordinary differential equations. The model is capable of generating realistic synthetic *ECG* signals in a 3D space (x,y,z). The peaks and troughs of the *ECG* signal, such as *P*, *Q*, *R*, *S*, and *T*, correspond to negative and positive Gaussian events in the z-direction.

* Corresponding author.
E-mail address: ruvazquez@ipn.mx (R. Vázquez-Medina).

https://doi.org/10.1016/j.compbiomed.2018.05.017
Received 15 February 2018; Received in revised form 15 May 2018; Accepted 15 May 2018

Gidea et al. [6] introduced three models of the electrical activity of the heart, transforming the model proposed by Ref. [12] into a discrete dynamical system by time-discretization. To generate quasi-periodic motion, similar to McSharry's model, the circle and standard maps are coupled with the discrete version of this model. Sadayi et al. [13] showed a modification of the McSharry's model assuming that their model may be effectively used to generate health *ECG*s as well as arrhythmias.

In some electrical models, the main pacemakers or the pacemakers and cardiac muscles represent the heart using Van der Pol (*VDP*) family oscillators. Particularly, the *VDP* oscillator can be viewed as an *RLC* oscillator with an active resistor, which introduces a nonlinearity in the system. The *VDP* oscillator has been used in the pioneering studies of heart electrical activity developed by Van der Pol and Van der Mark [14]. They applied the relaxation oscillation theory to the heartbeat by considering the heart to be a three-degree-of-freedom system consisting of the sino-atrial node, the atrium, and the ventricle. Thus, for the system emulation, they used three *VDP* oscillators coupled with time delays. In another related work, Gois and Savi [15] proposed a model to reproduce *ECG* signals from three modified *VDP* oscillators coupled with time delays. In their model, each oscillator represents a different natural pacemaker, which can produce pathological rhythms by varying parameters or changing the coupling. Kaplan et al. [16] associated the practical Wien Bridge (used as a wave rectifier) with the *VDP* family oscillators to propose a model to reproduce the electrical activity in the heart. Kaplan et al. [16] showed that two coupled Wien Bridge oscillators, with a time delay, could be used to generate *ECG* signals. In 2014, Ryzhii and Ryzhii proposed a model with physiological grounds [7], composed of two parts: the first considers the main pacemaker, SA node, and AV node and HP system; and the second describes both the atrial and ventricular muscles. The model allows for the generation of synthetic *ECG* signals as a combination of atrial and ventricular signals.

Heartbeat dynamics have been also modeled using tools such as neural networks and fractional order systems. Jafarnia-Dabanloo et al. [17] proposed a neural network to generate an *ECG* cycle, and by modifying the Zeeman's model [18], they produced an *RR*-tachogram, which includes the effects of the sympathetic and parasympathetic nervous system. Das and Maharatna [8] presented a modification of Kaplan's model, introducing a fractional-order model based on two filtered *VDP* oscillators. The motivation to explore fractional-order arises because the Kaplan's model does not have the capability to generate different *ECG* waveforms. As a result, they shown that various *ECG* signals can be simulated by changing the fractional order of the equation system.

Thus, most models that synthesize *ECG* signals are based on nonlinear oscillators (*VDP* oscillators). However, the proposed model is based on a network of two linear oscillators and a time delay to simulate signal propagation from atria to ventricles. In the proposed model, one oscillator simulates the electrical behavior of the atria and another simulates the behavior of the ventricles. Additionally, an external periodic signal influences the behavior dynamics of this network of linear oscillators. The frequency of this external signal is related to a healthy heart rate. Thus, we propose a periodically kicked network of two capacitively coupled linear oscillators to model the electrical activity of the heart, and we show that it can generate realistic synthetic *ECG* signals. Two capacitively coupled *RLC* electrical circuits compose the proposed model, where *R* stands for resistance, *L* for inductance, and *C* for capacitance. The capacitive-coupling can be either unidirectional or bidirectional. One *RLC* circuit represents the atria, another represents the ventricles, and the coupling-capacitor represents the electrical cardiac conduction between them. In addition, a time delay simulates the electrical propagation delay from atria to ventricles. In the proposed model, the network of linear oscillators is periodically kicked by the main pacemaker that introduces the periodic forcing of limit cycles into the system. Four linear differential equations represent the model, and they can be solved analytically when a single impulse is used as the oscillators' network input. By the superposition principle, the obtained solution can be extended when an impulse train is considered. The importance of the proposed model lies in its simplicity and linearity. In general, the analytical and numerical treatment of system behavior based on linear models is easier than using nonlinear models. Although nonlinear models are generally considered better approximators of the behavior of a system, the proposed model offers a sufficient approximation to the electrical behavior of a healthy heart.

In the proposed model, we use an external signal generator to influence the electrical behavior of the linear oscillator network and produce *ECG* signals of a healthy rhythm. This model feature and the internal parameters of the oscillators allow for the exploration of some pathological heart behaviors. To achieve this, as a first approximation, we considered a system should be built to generate reference signals that follow not only the cardiac frequency of the healthy behavior of a heart but also some possible pathological behaviors. This paper is organized as follows. In Section 2, some features of the kicked oscillators are mentioned. Furthermore, the proposed model is described using a block scheme. Then, the dynamics of a single *RLC* electrical circuit are discussed to relate the produced waveform with the depolarization and repolarization processes of the heart. Finally two linear oscillators are coupled by means of a capacitor C_X, and the *ECG* signal is obtained by the linear combination of the current in the inductors of each *RLC* circuit. In Section 3, the results of bidirectional and unidirectional coupling are presented and discussed; we show that both coupling options on the systems can model the electrical activity of the heart. In Section 4, *ECG* signals produced by the proposed model are compared with *ECG*s generated by the models reported by Kaplan. Section 5 presents the conclusion of the study.

2. Model

2.1. Kicked oscillator

The study of driven oscillators has a long history. In 1927, Van der Pol and Van der Mark, observed the dynamical behavior of electrical circuits exhibited stable oscillation when they were periodically forced [14]. In 1961, FitzHugh studied the response of the FitzHugh-Nagumo neuron model to external perturbations [19]. Since then, there have been several models of driven oscillators.

The kicked harmonic oscillator is a type of driven oscillator that has been useful in the area of quantum chaos and dynamical quantum localization [20]; it has been studied extensively in the last decade [21, 22]. Some authors have shown the *shear* feature as a property of the limit cycle that determines whether the kicked oscillator is stable or chaotic [21]. The periodically kicked oscillator has generated some interest for simulating low-dimensional systems like quantum wires, semiconductor superlattices or trapped ions [23,24]. Kicked oscillators are an example of kicked degenerate systems used to study chaos because they do not obey the Kolmogorov-Arnol'd-Moser theorem, which is related to the persistence of quasiperiodic motions under small perturbations and explains how the trajectory appearance of a system integrable under small perturbations is modified [25,26].

In congruence with the electrical modeling of heart activity proposed in this work, we restrict ourselves to a network of two identical linear oscillators that include a main pacemaker that produces periodic kicks, or forces that are turned on during short intervals. The basic equation considered in this work corresponds to the kicked harmonic damped oscillator, given as (1):

$$\ddot{x} + \alpha\dot{x} + \omega_0^2 x = Af(x)\sum_{n=1}^{\infty}\delta(t - nT), \tag{1}$$

where ω_0 is the natural frequency, α is the damping factor of the system, A is the amplitude of kicks, $f(x)$ is an arbitrary function of x, but not of t, and $\delta(t - nT)$ is an impulse displaced nT s.

Note that a linear, time-dependent driving term alters the orbits in the phase space of the system; if A and $f(x)$ are not equal to zero in (1), the system is non-autonomous and has more than one degree of freedom. Additionally, note that when $f(x) = 1$ or x, the solution of (1) is linear and invertible. In this way, no chaotic dynamics are expected of the system. Thus, choosing the driving term in Eq. (1) to be a sum of delta functions

allows us to obtain a solution to the differential equations for the kicked linear oscillator. Now, consider that $\Omega = 2\pi/T$ is the kick frequency and is equal to the natural frequency of the oscillator's energy if the oscillator becomes unbounded. This feature is called *resonance*, and it is a phenomenon occurring in many nonlinear systems, which leads to the destruction of the integrable behavior. Further, if the ratio (ω_0/Ω) is a rational number, then the system will return to its initial conditions and is periodic. If the ratio (ω_0/Ω) is an irrational number, quasiperidic oscillation can be expected.

2.2. General description of the model

A linear oscillator network alone cannot electrically represent the biological phenomena of the heart. However, its dynamical behavior can be enriched if it is periodically subjected to abrupt momentum transfers, in general, from its natural oscillation period. This feature in classical *RLC* oscillators can lead to new applications. To demonstrate the dynamical behavior of the proposed model, we use the macroscopic structure of the cardiac conduction system shown in Fig. 1, which constitutes the basis of the proposed model for generating *ECG* signals.

This macroscopic structure uses two capacitively coupled *RLC* electrical circuits to produce waveforms, such as the patterns (peaks and troughs) exhibited by the ECG signals, a pulse train related to the features (pulse width and frequency) of a cardiac signal, and a time delay to represent the electrical transport delay. Note that the time delay takes place at the boundary between the atria (*AT*) and ventricles (*VN*). In this context, we consider the depolarization and repolarization wave fronts in *AT* and *VN* as separate processes, where each one is represented by an *RLC* circuit. The atria *RLC* circuit is stimulated by an external electrical signal from the main pacemaker represented by the pulse train; then, it is synchronized to the ventricle *RLC* circuit using capacitive coupling. Using this description, the *AT* and *VN* electrical responses are modeled by a system of four linear ordinary differential equations, where the *ECG* signal is obtained by the sum of the currents in the inductors of each electrical circuit.

The detailed mathematical description of the current pulse stimulus (*SA*), excitable oscillators (*AT* and *VN*), and the coupling between them are described in the next subsections.

2.3. Single RLC circuit

Consider a single *RLC* parallel circuit with dynamics as described by the following state equations:

$$\begin{aligned} C\dot{V}_C(t) &= I(t) - I_L(t) - \frac{V_C(t)}{R}, \\ L\dot{I}_L(t) &= V_C(t), \end{aligned} \tag{2}$$

where $V_C(t)$ is the voltage of the capacitor and $I_L(t)$ is the currents of the inductors at time t. The dots in (2) denote differentiation with respect to time. $I(t) = A\sum_{n=1}^{\infty}\delta(t - nT)$ is an input driving signal (impulse train) that triggers the dynamics of the system. The electrical circuit described by (2) is shown in Fig. 2.

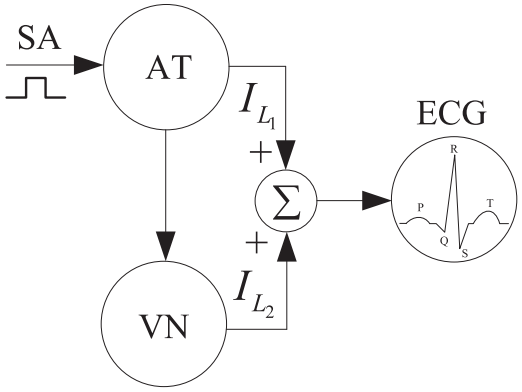

Fig. 1. General scheme of the proposed model.

Numerical simulations can be used to study the system dynamically, starting from a given initial condition or an external force. The evolution of the voltage in the capacitor and the current passing through the inductor can be described using either a time plot or a phase portrait. Both of them are shown in Fig. 3, using the parameter values: $I(t) = 0\ A$, $R = 1\ \Omega$, $L = 1\ mH$ and $C = 1\ mF$, with $V_C(0) = 1$ and $I_L(0) = 0$ as initial conditions. The time plot (left) shows the values of individual states as a function of time, that is, the current in the inductor (dashed line) and the voltage in the capacitor (solid line). The phase portrait (right) shows the vector field for (2) where a stable focus can be observed.

Now, let the $I(t)$ and $I_L(t)$ be the input and output currents in the inductor, respectively. The transfer function of the system (2) in the Laplace domain is then

$$\frac{I_L(s)}{I(s)} = \frac{\frac{1}{LC}}{s^2 + \frac{1}{RC}s + \frac{1}{LC}}. \tag{3}$$

The natural frequency ω_0 and the damping factor α can be obtained easily from (3).

$$\alpha = \frac{1}{RC}, \tag{4a}$$

$$\omega_0 = \sqrt{\frac{1}{LC}}. \tag{4b}$$

The impulse response of system (3) with amplitude A is given by

$$I_1(t) = \frac{A\gamma\omega_0^2 e^{-\frac{\alpha+\sqrt{\alpha^2-4\omega_0^2}}{2}t}\left(e^{t\sqrt{\alpha^2-4\omega_0^2}} - 1\right)}{\sqrt{\alpha^2 - 4\omega_0^2}}, \tag{5}$$

where γ refers to the input pulse width. It is known that in numerical simulations, as well as in real experiments, ideal impulses can only be approximated as pulses of a given width. The pulse width should be smaller than the period of the oscillator, that is, $\gamma \ll \frac{2\pi}{\omega_0}$.

We found that the impulse response of the system (3), that is, the current in the inductor (shown by a dashed line in Fig. 3), is quite similar to the response exhibited by the modified FitzHugh-Nagumo model [27] (see Fig. 4). Such a model is commonly used to explain the basic mechanisms of excitability phenomena in biological media.

In fact, Ryzhii and Ryzhii [7] used the FitzHugh-Nagumo model to describe the depolarization and repolarization processes in cardiac muscles. The similarity between the impulse response of system (3) and the one produced by a modified FitzHugh-Nagumo model lead us to propose that *RLC* electrical circuits can provide a simple way to model the depolarization and repolarization processes in atria and ventricles to describe the electrical activity in the heart.

2.4. Capacitively coupled RLC circuits

Next, consider two parallel *RLC* circuits with resistance R_i, inductance L_i and capacitance C_i with $i = 1, 2$, coupled by a capacitor with

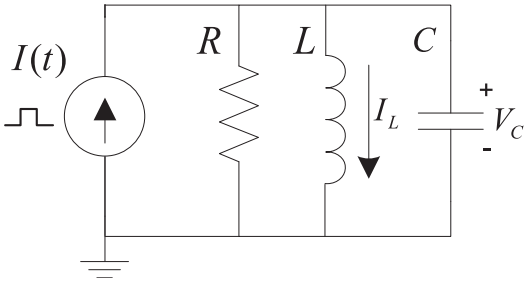

Fig. 2. Single RLC parallel circuit.

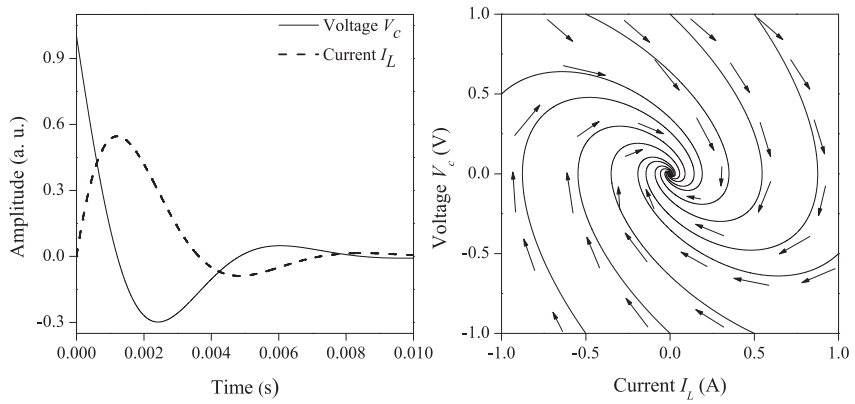

Fig. 3. Time series (left) and phase portrait (right) of the model (2) using the parameters $I(t) = 0\ A$, $R = 1\Omega$, $L = 1mH$ and $C = 1\ mF$, with $V_C(0) = 1$ and $I_L(0) = 0$ as initial conditions.

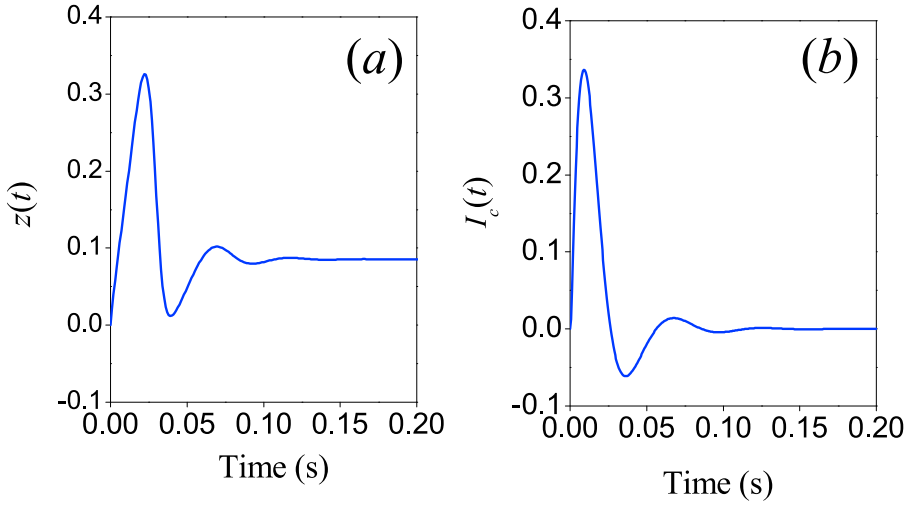

Fig. 4. Impulse response of the (a) FitzHugh-Nagumo oscillator and (b) *RLC* linear oscillator.

capacitance C_X (see Fig. 5). $I(t)$ is an input driving signal characterized by a current impulse train. Taking into account the similarity, discussed above, of the waveforms generated for an *RLC* circuit with the waveform of depolarization and repolarization processes of the heart, we consider the description of electrical responses of the atria and ventricles as separate processes, each one represented by a *RLC* circuit. The stimulation impulses provided by an external current source represent the global effects of the trans-membrane ionic current generated by the main pacemaker (*SA* node). The capacitor provides the coupling between the atria and ventricles and represents the electrical conduction system.

If the current in the inductors $I_{Li}(t)$ and the voltage in the capacitors $V_{Ci}(t)$ $(i = 1, 2)$ are used as state variables, the equations that describe the system in Fig. 5 are:

$$C_1\dot{V}_{C1}(t) = I(t) - I_{L1}(t) - \frac{V_{C1}(t)}{R_1} - C_X\left(\dot{V}_{C1}(t) - \dot{V}_{C2}(t)\right), \tag{6a}$$

$$L_1\dot{I}_{L1}(t) = V_{C1}(t), \tag{6b}$$

$$C_2\dot{V}_{C2}(t) = -I_{L_2}(t) - \frac{V_{C2}(t)}{R_2} + C_X\left(\dot{V}_{C1}(t) - \dot{V}_{C2}(t)\right), \tag{6c}$$

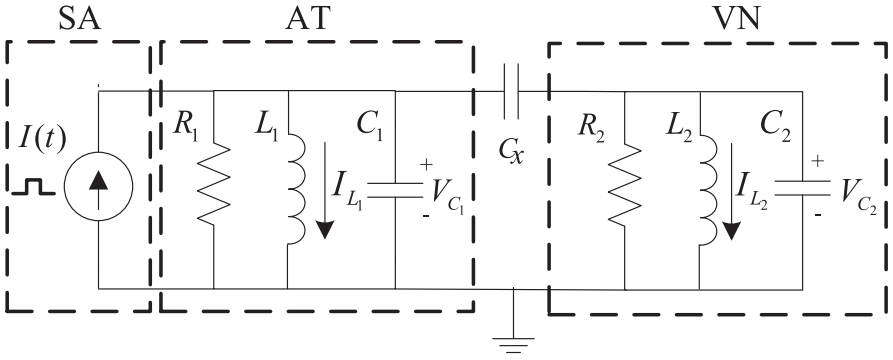

Fig. 5. Two linear RLC electrical circuits coupled by a capacitor.

$$L_2\dot{I}_{L2}(t) = V_{C2}(t), \tag{6d}$$

where $I(t) = A\sum_{n=1}^{\infty}\delta(t-nT)$, where A is the magnitude of each pulse and T is the interval between start of each pulses.

The current impulses act as an initial condition of the network where, as stated above, the impulse width should be smaller than the period of the system (in this case approximately 700 times smaller). The frequency of the pulses and the natural frequency of the oscillators define the cardiac frequency. These current impulses are introduced in the first *RLC* oscillator to model the electrical response of the atria. A second oscillator models the response of the ventricles and is stimulated by the signal transferred through the coupling capacitor.

System (6) can be transformed into a couple of second-order differential equations for variables I_{L1} and I_{L2}. In the Laplace transform space and by considering two identical oscillators ($R = R_1 = R_2$, $C = C_1 = C_2$ and $L = L_1 = L_2$), the couple of second-order differential equations ($\ddot{I}_{L1}\ddot{I}_{L2}$) becomes:

$$s^2\tilde{I}_{L1} + \alpha s\tilde{I}_{L1} + \omega^2\tilde{I}_{L1} = \omega^2 I(s) - Ws^2\left(\tilde{I}_{L1} - \tilde{I}_{L2}\right), \tag{7a}$$

$$s^2\tilde{I}_{L2} + \alpha s\tilde{I}_{L2} + \omega^2\tilde{I}_{L2} = Ws^2\left(\tilde{I}_{L1} - \tilde{I}_{L2}\right), \tag{7b}$$

where $\tilde{I}_{Li} = I_{Li}(s)$, with $i = 1, 2$, $\alpha = 1/RC$, $\omega_0^2 = 1/LC$ and $W = C_X/C$.

Additionally, note that $F(s,\alpha,\omega_0)\tilde{I} = \tilde{I}_{L1} + \tilde{I}_{L2}$ and $F(s,\alpha_x,\omega_{0x})\tilde{I} = \tilde{I}_{L1} - \tilde{I}_{L2}$, where $\alpha_x = 1/(R(C+2C_X))$, $\omega_{0x}^2 = 1/(L(C+2C_X))$ and $F(s,\alpha,\omega_0) = \omega_0^2/(s^2+\alpha s+\omega_0^2)$. Now, solving (7a) and (7b) for $\tilde{I}_{L1}$ and $\tilde{I}_{L2}$,

$$\tilde{I}_{L1} = \frac{F(s,\alpha,\omega_0) + F(s,\alpha_x,\omega_{0x})}{2}I(s), \tag{8a}$$

$$\tilde{I}_{L2} = \frac{F(s,\alpha,\omega_0) - F(s,\alpha_x,\omega_{0x})}{2}I(s), \tag{8b}$$

Thus, applying inverse Laplace transform to (8a) and (8b), $I_{L1}(t)$ and $I_{L2}(t)$ can be obtained.

Now, considering that the current in the inductor in an *RLC* oscillator (see subsection 2.3) is quite similar to the response exhibited by the modified FitzHugh-Nagumo, the synthetic *ECG* waveform is calculated as a composition of the signals from *AT* and *VN* represented by the current in the inductors. A time delay τ has been introduced in I_{L1} to keep the correct arrangement in the waveform of the *ECG* signal, that is, the *P* wave in the first place and the *QRS* complex and *T* wave in the second place. Therefore, (9) produces the *ECG* signal:

$$ECG(t) = \beta_1 I_{L1}(t-\tau) + \beta_2 I_{L2}(t), \tag{9}$$

where β_1 and β_2 are scaling factors introduced to match the generated *ECG* signal with physiologically measured amplitudes. In a similar way, it is possible to define:

$$\frac{d}{dt}ECG(t) = \frac{\beta_1}{L_1}V_{C1}(t-\tau) + \frac{\beta_2}{L_2}V_{C2}(t). \tag{10}$$

The method used to fit the parameters on (9) is the *perceptron*, which is based on the supervised learning algorithm developed by Frank Rosenblatt [28,29]. This algorithm is a type of artificial neural network that can be used as a linear sorter. Before starting the classification process, the *perceptron* is submitted to a learning stage, which consists of adjusting the parameters of each I_{Li} ($i = 1, 2$) based on the difference between the obtained signal and the desired signal. Novikoff [30,31] proved that the learning algorithm converges after a finite number of iterations.

We exported the ideas of the learning stage of the perceptron to fit the weights of the linear sum on (9) to obtain the *ECG* signal. Thus, $ECG_r(t) \in [a,b]$ is the real *ECG* signal, $ECG_e(t) \in [a,b]$ is the estimated *ECG* signal obtained from linear sum on (9), $\beta_1(n)$ and $\beta_2(n)$ are the weights at the iteration n, γ is the convergence rate and ε is the specified error threshold.

Thus, the fitting process is as follows:

1. Initialize $\beta_1(n)$ and $\beta_2(n)$ as random values.
2. Calcule the actual $ECG_e(t)$ according to (9).
3. Obtain the error of estimation $e(t) = ECG_r(t) - ECG_e(t)$.
4. Update the parameters $\beta_1(n)$ and $\beta_2(n)$ according to:

$$\beta_i(n+1) = \beta_i(n) + \gamma\int_a^b e(t)I_{Li}(t)$$

where $i = 1, 2$.

5. Steps 2, 3, and 4 may be repeated until the error integrals are less than ε, that is:

$$\int_a^b e(t)I_{Li}(t) \le \varepsilon$$

2.5. Coupled RLC circuits by a unidirectional capacitor

In a single oscillator, the stored and dissipated energy can be traced easily and an analytical solution can be obtained. However, when two *RLC* oscillators are coupled, the analytical treatment is generally cumbersome because it implies solving a fourth-order system. To simplify the analysis, we consider only unidirectional coupling, which can be justified as follows. Because oscillator-1 receives the signal excitation, its own resistor dissipates a portion of the initial energy and oscillator-2 receives the remaining energy using the coupling capacitor. In a similar way, oscillator-2 dissipates energy owing to its resistor and the remaining energy is returned to oscillator-1. We noticed that this returned energy does not produce significant effects on the *ECG* waveform; thus, the effect of the returned energy can be dismissed and a unidirectional coupling, where the energy flows from atria (oscillator-1) to ventricles (oscillator-2), can be assumed. It is important to mention that both cases, unidirectional and bidirectional coupling, can generate *ECG* signals, but only unidirectional coupling is highlighted owing to the mathematical simplification it offers when the analytical solution is obtained.

If we consider unidirectional coupling, the term $C_X(\dot{V}_{C1}(t) - \dot{V}_{C2}(t))$ in (6a) is dropped:

$$C_1\dot{V}_{C1}(t) = A\sum_{n=1}^{\infty}\delta(t-nT) - I_{L1}(t) - \frac{V_{C1}(t)}{R_1}, \tag{11a}$$

$$L_1\dot{I}_{L1}(t) = V_{C1}(t), \tag{11b}$$

$$C_2\dot{V}_{C2}(t) = -I_{L_2}(t) - \frac{V_{C2}(t)}{R_2} + C_X\left(\dot{V}_{C1}(t) - \dot{V}_{C2}(t)\right), \tag{11c}$$

$$L_2\dot{I}_{L2}(t) = V_{C2}(t). \tag{11d}$$

A mathematical analysis supported by a block diagram estimates the influence of the coupling term. Fig. 6(*a*) shows the block diagram of system (6), where $C_X(\dot{V}_{C1}(t) - \dot{V}_{C2}(t))$ in (6a) has been highlighted (red block) to make evident the feedback from oscillator-2 to oscillator-1.

In Fig. 6, $F_1(s)$ and $F_2(s)$ correspond to the transfer functions of atria (oscillator-1) and ventricles (oscillator-2), respectively:

$$F_1(s) = \frac{I_{L1}(s)}{I(s)} = \frac{\frac{1}{L_1C_1}}{s^2 + \frac{1}{R_1C_1}s + \frac{1}{L_1C_1}},$$
$$F_2(s) = \frac{I_{L2}(s)}{U(s)} = \frac{\frac{1}{L_2C_2}}{s^2 + \frac{1}{R_2C_2}s + \frac{1}{L_2C_2}}. \tag{12}$$

Assuming unidirectional coupling, simple algebra of blocks can be

applied to the diagram in Fig. 6(*a*). In this way, I_{L1} is the input of the second oscillator (see Fig. 6(*b*)). Now, by considering two identical oscillators ($R = R_1 = R_2$, $C = C_1 = C_2$ and $L = L_1 = L_2$), (13) produces the transfer function I_{L2}/I_{L1}:

$$G_1(s) = \frac{I_{L2}(s)}{I_{L1}(s)} = \frac{\frac{C_X s^2}{C+C_X}}{s^2 + \frac{1}{R(C+C_X)}s + \frac{1}{L(C+C_X)}}. \tag{13}$$

Now, two transfer functions in cascade are obtained; these, cascaded systems can be analyzed and solved sequentially. Thus, two solutions can be calculated independently. First, the solution for I_{L1} was obtained in (5) and such solution is used as the input of $G_1(s)$. From this input, it is easy to compute the solution for I_{L2}:

$$I_2(t) = A\gamma\omega_0^2\left[\frac{2e^{\left(-\frac{\alpha}{2}\right)t}\sinh\left(\frac{\sqrt{\alpha^2-4\omega_0^2}}{2}t\right)}{\sqrt{\alpha^2-4\omega_0^2}} - \frac{2e^{\left(-\frac{\alpha}{2(1+C_X\omega_0)}\right)t}\sinh\left(\frac{\sqrt{\alpha^2-4\omega_0^2(1+C_X\omega_0)}}{2(1+C_X\omega_0)}t\right)}{\sqrt{\alpha^2-4\omega_0^2(1+C_X\omega_0)}}\right], \tag{14}$$

where α and ω_0 are given by (4a) and (4b), respectively.

Then, we use (9) to compute the *ECG* signal produced by two *RLC* oscillators coupled by a unidirectional capacitor. Note that (5) must be delayed by τ s; this time delay represents the electrical transport delay that take place in an electrical conduction realistic system. The *ECG* signal can be obtained by:

$$ECG(t) = 2A\gamma\omega_0^2\left[\frac{e^{-\frac{\alpha+\sqrt{\alpha^2-4\omega_0^2}}{2}u(t-\tau)}\left(e^{(t-\tau)\sqrt{\alpha^2-4\omega_0^2}}-1\right)u(t-\tau)}{\sqrt{\alpha^2-4\omega_0^2}} + \frac{e^{\left(-\frac{\alpha}{2}\right)t}\sinh\left(\frac{\sqrt{\alpha^2-4\omega_0^2}}{2}t\right)}{\sqrt{\alpha^2-4\omega_0^2}} - \frac{e^{\left(-\frac{\alpha}{2(1+C_X\omega_0)}\right)t}\sinh\left(\frac{\sqrt{\alpha^2-4\omega_0^2(1+C_X\omega_0)}}{2(1+C_X\omega_0)}t\right)}{\sqrt{\alpha^2-4\omega_0^2(1+C_X\omega_0)}}\right]. \tag{15}$$

where $u(t-\tau)$ is the Heaviside step function given by

$$u(t-\tau) = \begin{cases} 0 & t < \tau \\ 1 & t \geq \tau \end{cases} \tag{16}$$

In addition, it is important to remark that (15) is the solution for a single impulse, which produces a single *ECG* cycle. As it occurs in the heart, a periodic stimulus (pulse train) should be considered to represent the successive relaxation and contraction of the cardiac muscles to obtain an *ECG* signal. As $I(t)$ in (11a) corresponds to a series of impulses displaced nT s, we obtained the solution of (11) for a single impulse; then, applying the superposition principle, we extended the solution to a train of impulses. The electrical stimulation from main pacemaker is a periodic signal where each relaxation and contraction of cardiac muscles is a version similar to the procedure that occurs in the heart. This phenomenon can be clearly observed in the periodicity in the *ECG* signal.

3. Results

To show the behavior dynamics of the proposed model, different plots of (9) for bidirectional and unidirectional couplings are considered. Both cases were analytically solved in Sections 2.4 and 2.5, respectively. The R, C, L, and C_X parameters were adjusted to qualitatively match duration times of the intervals of a healthy *ECG* signal. Under this consideration, the following parameters are adopted for normal heart functioning: $R_1 = R_2 = 1\ \Omega$, $L_1 = L_2 = 22.2\ mH$, $C_1 = C_2 = 22.2\ mF$ and $C_X = 11.11\ mF$. With these parameter values, we obtained the duration times denoted in Table 1, which are within the reference times reported in international databases [32].

The *PR* interval corresponds to *AV* nodal delay, that is, the propagation time of the electrical impulse from the *SA* node to the ventricles. Note that the time delay introduced in our model is directly related with the *PR* interval, which in normal values lies between 0.12 and 0.20 s. We set the time delay to $\tau = 0.12\ s$. It is important to mention that an automatic determination of the system parameters is beyond the scope of this contribution; we are interested in qualitative system response.

The stimulation current pulses $I(t)$ are characterized by a pulse train with a pulse duration of 200 μs, an amplitude of 5 A and a frequency of 1.125 Hz injected in atria (oscillator-1), which defines the heart rate corresponding to a sinus rhythm close to 70 bpm. Note that the pulse width of the driving force is smaller than the period of the oscillator ($T_{osc} = 0.139$ s), about 700 times. Here, $I(t)$ shoots the dynamics of the system; therefore, we set initial conditions to zero, that is, $V_{C1}(0) = 0$, $V_{C2}(0) = 0$, $I_{L1}(0) = 0$ and $I_{L2}(0) = 0$.

To derive the constants (β_1, β_2), a supervised learning algorithm

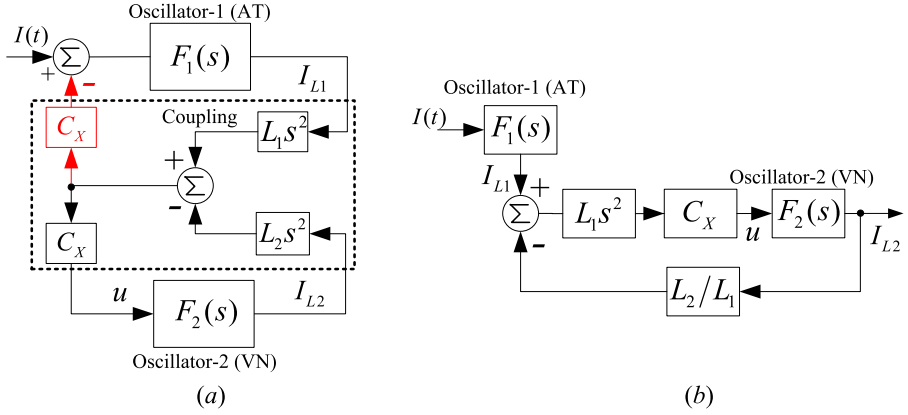

Fig. 6. Block diagrams: (*a*) two linear *RLC* electrical circuits coupled by a capacitor. The coupling from *VN* to *AT* is highlighted with the red block, (*b*) two linear *RLC* oscillators with a unidirectional coupling. (For interpretation of the references to colour in this figure legend, the reader is referred to the Web version of this article.)

Table 1
Normal electrocardiography intervals.

Intervals	Reference Time (ms)	Obtained Time (ms)
P wave	< 120	50
QT interval	> 350	380
QRS complex	$70 - 100$	88

called perceptron, described in Section 2.4, was used. The *ECG* signals presented in this Section were obtained from (9) with $\beta_1 = 1.5$ and $\beta_2 = 0.7$.

Fig. 7 shows the resulting *ECG* signals and corresponding responses from the *AT* and *VN* muscles generated by the proposed model considering both couplings: unidirectional and bidirectional. Fig. 7(a) shows the *AT* and *VN* responses corresponding to a unidirectional coupling and for the bidirectional case, Fig. 7(b) shows the electrical responses of the muscles. In both figures, the dashed line denotes the current passing through the inductor of oscillator-1 and the solid line corresponds to the current in the inductor of oscillator-2, which represent the *VN* and *AT* responses, respectively. The main idea is building the *ECG* waveform from composition of these signals. Fig. 7(c) shows a comparison of the total *ECG* waveform for the unidirectional (green line) and bidirectional (blue line) coupling. In both cases, the waveforms generated for a normal rhythm (60–70 bpm) present the representative details and the most important waves (P, QRS, T) of a typical *ECG* signal. That is, our model can capture the general behavior of real *ECG*s. There is no substantial

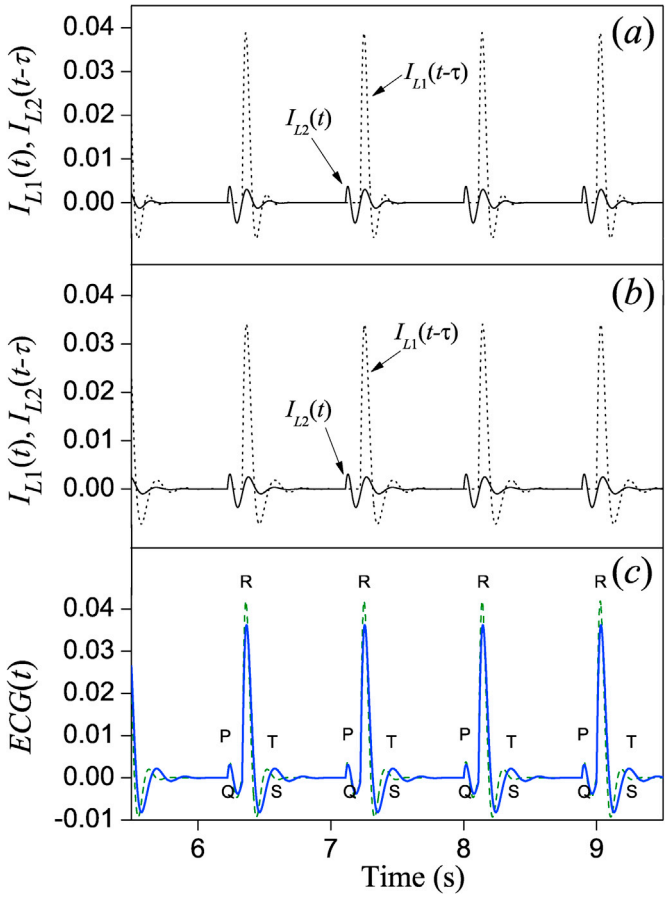

Fig. 7. Atrial (solid line) and ventricular (dotted line) response obtained, considering: (a) unidirectional coupling and (b) bidirectional coupling. (c) *ECG* waveform produced by the proposed model with unidirectional (dashed green line) and bidirectional (solid blue line) coupling. (For interpretation of the references to colour in this figure legend, the reader is referred to the Web version of this article.)

change in the *ECG* waveform when a unidirectional or bidirectional coupling is chosen, therefore, from now, for simplicity, we only concentrate in the unidirectional coupling.

In Fig. 8, two types of the phase plots are drawn for a unidirectional coupling between the oscillators. In Fig. 8(a), a noticeable limit cycle or closed orbit corresponding to *ECG* versus $\frac{d}{dt}ECG$ can be observed. A periodic behavior is the natural state of the heart. Fig. 8(b) shows the phase planes of the current versus the voltage of each oscillator. The green line corresponds to the *AT* response represented by oscillator-1, and the blue line denotes the *VN* response modeled by oscillator-2. The phase plane of Fig. 8(a) is the result of the sum of the phase planes of the individual oscillators (Fig. 8(b)).

After getting normal *ECG* as a reference, we have plotted the *AT* and *VN* responses for two different values of ω_0 and α to discuss the effects of these parameters on the oscillators. For this, the τ, C_X, β_1 and β_2 parameters, the initial conditions, and the stimulation current pulses stay at the same values for normal rhythm. At first, we consider the case where the natural frequency changes. Here, L and C are changed in the same proportion and R is fixed to 1Ω. Fig. 9(a) and Fig. 9(b) show the *AT* and *VN* responses, respectively, for two pairs of values: $L = 44.4$ *m*H and $C = 44.4$ *m*F (blue lines) and $L = 11.1$ *m*H and $C = 11.1$ *m*F (red lines). For comparison purposes, we have include the values used for a normal rhythm: $L = 22.2$ *m*H and $C = 22.2$ *m*F (green lines). As expected, the variation in ω_0 produces noticeable changes in the period and slight changes in the damping term. These alterations suggest effects that can be used to simulate some heart pathologies related with the heart rate, for example, sinus tachycardia, which a fast rhythm greater than 100 bpm, or sinus bradycardia, which is a slow rhythm less than 60 bpm; both have small variations in the waveform.

In second place, we fix $L = 22.2$ *m*H and $C = 22.2$ *m*F, and change R to move the damping factor. In Fig. 10(a) and Fig. 10(b), the *AT* and *VN* responses are drawn, respectively, for three different values of R. The green curves denote the value used for the sinus rhythm, i.e., $R = 1\,\Omega$, the blue line belongs to $R = 0.5\,\Omega$ and the red line refers to $R = 2\,\Omega$. From the figures, we observe an increase in the oscillations for R less than reference value and an attenuation when R is greater. Therefore, in first instance, by changing R, we can produce the absence or excess of important waves, such as the *P*-wave or *T*-wave.

It is important to mention that the previous study was a preliminary revision of the variation in some parameters and only represented an initial idea to suggest that proposed model can be used to simulate some disturbances of the cardiac rhythm. It is beyond the scope of the present work to perform a detailed analysis of parameter effects; investigation is required for further work, which will be reported in future work.

4. Discussion

This section presents a comparison of the proposed model against the models proposed by Ref. [16]. In Ref. [16], the practical Wien Bridge (WB) relates to a family of *VDP* oscillators, which are used as half wave rectifiers with a low pass filter, also known as Filtered *VDP* oscillator. It is shown that an *ECG*-like waveform can be generated using these types of oscillators. The authors propose two ways to generate *ECG* signals. The first model (three nonlinear differential equations) is a version of the WB oscillator. Two WB oscillators coupled with a time delay represent the second model (six nonlinear differential equations). Here, we reproduce numerical calculations of both models using a fourth order Runge-Kutta algorithm with fixed step $\Delta t = 0.01$, initial conditions: $x_0 = [0 \quad 10^{-6} \quad 0]^T$ and $x_0 = [0 \quad 10^{-6} \quad 0 \quad 0 \quad 10^{-6} \quad 0]^T$ for the first and second model, respectively, and the following parameters: $\varepsilon = 2$, $\mu = 1$, $\alpha = 0.05$. For the WB single, $T = 20$ was used and for the case of two coupled WB, $T = 30$ was used. In the results presented in this section, we plotted the first state variable of each filtered *VDP* oscillators for both cases, single WB and two coupled WB.

Fig. 11 shows time series of *ECG* signals generated by the Kaplan's

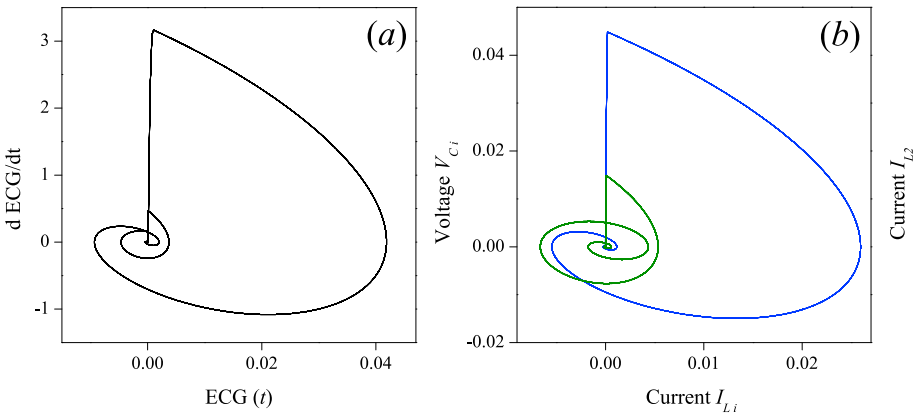

Fig. 8. Phase plane for the model (11): (a) ECG versus $\frac{d}{dt}ECG$. (b) Current in the inductor $I_{Li}(t)$ versus the voltage in the capacitor $V_{Ci}(t)$ for the atrial response (green line) with $i = 1$, and for the ventricular response (blue line) with $i = 2$. (For interpretation of the references to colour in this figure legend, the reader is referred to the Web version of this article.)

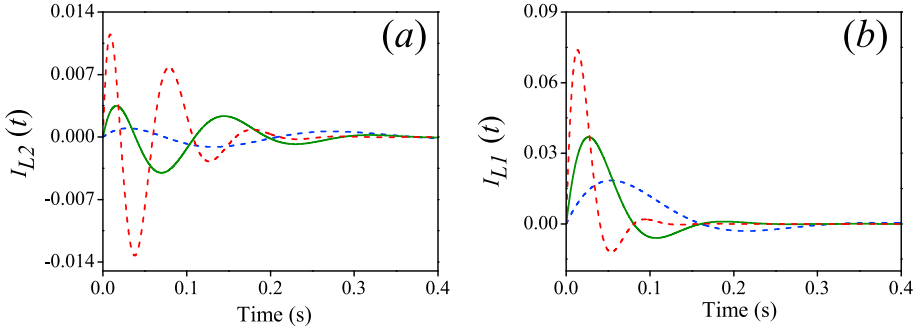

Fig. 9. Time series of AT and VN responses for $R = 1$ Ω and two values of L and C: blue line - $L = 44.4$ mH and $C = 44.4$ mF and red line - $L = 11.1$ mH and $C = 11.1$ mF. The green line corresponds to the values used for the normal rhythm: $L = 22.2$ mH and $C = 22.2$ mF. (a) Atria responses and (b) ventricles responses. (For interpretation of the references to colour in this figure legend, the reader is referred to the Web version of this article.)

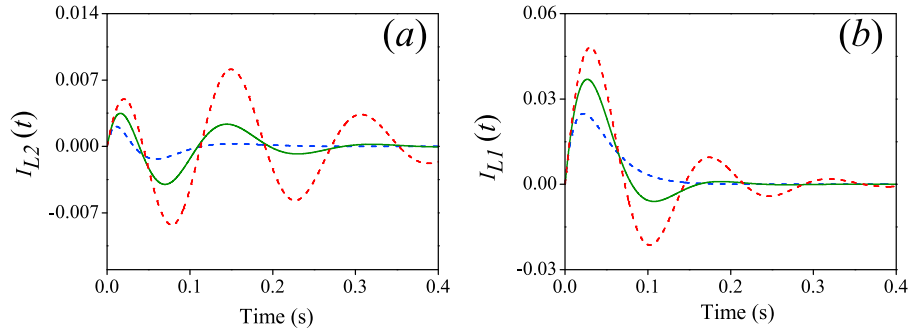

Fig. 10. Time series of AT and VN responses for $L = 22.2$ mH and $C = 22.2$ mF and two values of R: blue line $R = 2\Omega$ and red line $R = 0.5$ Ω. The green line corresponds to the values used for the normal rhythm: $R = 1$ Ω. (a) Atria responses and (b) ventricles responses. (For interpretation of the references to colour in this figure legend, the reader is referred to the Web version of this article.)

models and the proposed model. Fig. 11(a) shows an *ECG* waveform generated by the single WB single. Two distinct wave patterns can be distinguished; they have similar shape, but with different amplitude, even when the waveform is similar to an *ECG* signal. A real *ECG* only presents one pattern. However, Fig. 11(b) shows that the tiny beats vanish when two coupled WBs are coupled. Although, the *QRS* complex is prominent and *P* and *T* waves are absent. For its part, Fig. 11(c) shows the generated *ECG* from our model, which clearly presents the most important waves (*P*, *QRS*, and *T*) and contains the representative details of a healthy *ECG* signal. We believe that this comparison is interesting because all presented *ECG* signals were generated from models that describe electrical circuits: wave rectifiers in the case of Kaplan's models and *RLC* circuits in our case. However, in terms of complexity, our model is much simpler.

5. Conclusions

In this work, a mathematical model based on a periodically kicked network with two capacitively coupled linear electrical circuits is proposed to reproduce realistic *ECG* signals. Capacitive coupling can be either unidirectional or bidirectional. We used two *RLC* oscillators to represent the atrial and ventricular electrical responses, where a capacitor provides the coupling between them. An electrical pacemaker signal stimulates the atria *RLC* circuit. An impulse train of a specific width and frequency related to the cardiac signal represents the pacemaker signal. Thus, a linear combination of the current signals of each oscillator

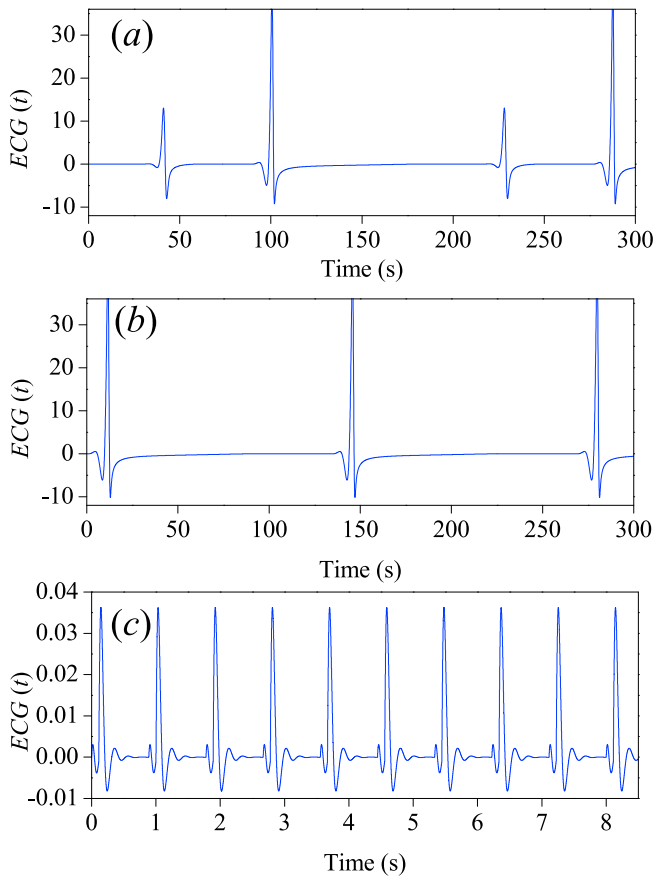

Fig. 11. *ECG* time series generated for: (*a*) a version of the WB oscillator, (*b*) two coupled WB oscillators and (*c*) the proposed model.

produces synthetic healthy *ECG* signals. To represent the electrical transport delay from atria to ventricles the first oscillator has a time delay. An analytical solution can be obtained when a single impulse is considered and by the superposition principle, the solution was extended to an impulse train, which introduces the periodic forcing of limit cycles in same manner that occurs in the heart. The obtained results show that the proposed model provides a simple way to model the global effects of cardiac electrical activity. The possibility of analytical solutions is an important feature of the proposed model. Furthermore, it is possible to study some effects of the system parameters, such as the interaction between excitable oscillators, the frequencies and coupling types, and the characteristics of main pacemaker to produce some non-healthy cardiac rhythm. Finally, a comparison with other models shows that our model can capture typical details and reproduce the most important waves exhibited by real *ECG*s.

Conflicts of interest

No conflict of interest.

Acknowledgements

RVM thanks financial support from IPN-México, through grant SIP-IPN-20181398. OJR acknowledges financial support from IPN-México, through grant SIP-IPN-20182124. JLA, RVM, OJR and MAQJ, acknowledge financial support from UNAM-DGAPA-PAPIIT and through grant IN110817.

References

[1] M.M. Elshrif, Shi Pengcheng, E.M. Cherry, Electrophysiological properties under heart failure conditions in a human ventricular cell: a modeling study, in: 2014 36th Annual International Conference of the IEEE Engineering in Medicine and Biology Society vol 2014, 2014, pp. 4324–4329, https://doi.org/10.1109/EMBC.2014.6944581. http://ieeexplore.ieee.org/document/6944581/%5Cnhttp. www.ncbi.nlm.nih.gov/pubmed/25570949.

[2] B.M. Rocha, E.M. Toledo, L.P. Barra, R.W. Dos Santos, An electromechanical left ventricular wedge model to study the effects of deformation on repolarization during heart failure, BioMed Res. Int. (2015), https://doi.org/10.1155/2015/465014.

[3] V. Urmaliya, G. Franchelli, A Multidimensional Sight on Cardiac Failure: Uncovered from Structural to Molecular Level, 2017, https://doi.org/10.1007/s10741-017-9610-y.

[4] J.P. Keener, J. Sneyd, Mathematical Physiology II: Systems Physiology, 2nd Edition, Vol. 8 of Interdisciplinary Applied Mathematics, Springer-Verlag, New York, 2008.

[5] J. Hurst, V. Fuster, R.A. Walsh, Hurst's the Heart, McGraw-Hill Medical, 2011.

[6] M. Gidea, C. Gidea, W. Byrd, Deterministic models for simulating electrocardiographic signals, Commun. Nonlinear Sci. Numer. Simulat. 16 (10) (2011) 3871–3880, https://doi.org/10.1016/j.cnsns.2011.01.022.

[7] E. Ryzhii, M. Ryzhii, A heterogeneous coupled oscillator model for simulation of ecg signals, Comput. Meth. Progr. Biomed. 117 (1) (2014) 40–49.

[8] S. Das, K. Maharatna, Fractional dynamical model for the generation of ECG like signals from filtered coupled Van-der Pol oscillators, Comput. Meth. Progr. Biomed. 112 (3) (2013) 490–507, https://doi.org/10.1016/j.cmpb.2013.08.012.

[9] A. Quarteroni, T. Lassila, S. Rossi, R. Ruiz-Baier, Integrated Heart–Coupling multiscale and multiphysics models for the simulation of the cardiac function, Comput. Meth. Appl. Mech. Eng. 314 (2017) 345–407, https://doi.org/10.1016/j.cma.2016.05.031.

[10] N. Zemzemi, R. Turpault, Y. Coudière, A. Azzouzi, A mathematical model of the Purkinje-Muscle Junctions, Math. Biosci. Eng. 8 (4) (2011) 915–930, https://doi.org/10.3934/mbe.2011.8.915. http://www.aimsciences.org/journals/displayArticlesnew. jsp?paperID=6448.

[11] P.C. Franzone, L.F. Pavarino, S. Scacchi, Mathematical Models of Cellular Bioelectrical Activity, in: Mathematical Cardiac Electrophysiology, Springer, 2014, pp. 21–75.

[12] P.E. McSharry, G.D. Clifford, L. Tarassenko, L.A. Smith, A dynamical model for generating synthetic electrocardiogram signals, Biomed. Eng. IEEE Trans. 50 (3) (2003) 289–294.

[13] O. Sayadi, M.B. Shamsollahi, G.D. Clifford, Synthetic ECG generation and Bayesian filtering using a Gaussian wave-based dynamical model, Physiol. Meas. 31 (10) (2010) 1309–1329, https://doi.org/10.1088/0967-3334/31/10/002.

[14] B. van der Pol, J. van der Mark, Frequency demultiplication, Nature 120 (1927) 363–364, https://doi.org/10.1007/978-0-387-79388-7, arXiv:1406.6401, https://books.google.com/books?id=HIkZ3QHbpTQC&pgis=1.

[15] S.R. Gois, M. a. Savi, An analysis of heart rhythm dynamics using a three-coupled oscillator model, Chaos, Solit. Fractals 41 (5) (2009) 2553–2565, https://doi.org/10.1016/j.chaos.2008.09.040. https://doi.org/10.1016/j.chaos.2008.09.040.

[16] B.Z. Kaplan, I. Gabay, G. Sarafian, D. Sarafian, Biological applications of the "filtered" van der pol oscillator, J. Franklin Inst. 345 (3) (2008) 226–232.

[17] N. Jafarnia-Dabanloo, D.C. McLernon, H. Zhang, A. Ayatollahi, V. Johari-Majd, A modified Zeeman model for producing HRV signals and its application to ECG signal generation, J. Theor. Biol. 244 (2) (2007) 180–189, https://doi.org/10.1016/j.jtbi.2006.08.005.

[18] E.C. Zeeman, Differential equations for the heartbeat and nerve impulse, Towards a theoretical biology 4(8).

[19] R. FitzHugh, Impulses and physiological states in theoretical models of nerve membrane, Biophys. J. 1 (1961) 445–466, https://doi.org/10.1007/978-0-387-79388-7, arXiv:1406.6401, https://books.google.com/books?id=HIkZ3QHbpTQC&pgis=1.

[20] G. Casati, B. Chirikov, J. Ford, F. Izrailev, Stochatic behaviour in Classical and Quantum Hamiltonian Systems, in: Ch. Stochastic Behaviour of a Quantum Pendulum under a Periodic Perturbation, vol 93, Springer, Berlin, 1979, pp. 334–352, https://doi.org/10.1007/978-0-387-79388-7. URL https://books.google.com/books?id=HIkZ3QHbpTQC&pgis=1.

[21] K. Lin, Y. Lai-Sang, Dynamics of periodically kicked oscillators, J. Fixed Point Theory Appl. 7 (2010) 291–312, https://doi.org/10.1016/j.cmpb.2013.08.012.

[22] R. Haiduc, Horseshoes in the forced van der pol system, Nonlinearity 22 (2009) 213–237, https://doi.org/10.1016/j.cmpb.2013.08.012.

[23] S. Gardiner, J. Cirac, P. Zoller, Quantum chaos in an ion trap: the delta-kicked harmonic oscillator, Phys. Rev. Lett. 79 (24) (1997) 4790–4793, https://doi.org/10.1016/j.cmpb.2013.08.012.

[24] R. Artuso, L. Rebuzzini, Nonlinearity effects in the kicked oscillator, Phys. Rev. E 66 (1) (2002) 017203–017206.

[25] C.E. Wayne, An introduction to kam theory (Jan. 2008) [cited September 25, 2017]. URL http://math.bu.edu/people/cew/preprints/introkam.pdf.

[26] D. Treschev, O. Zubelevich, Introduction to the perturbation theory of Hamiltonian systems, springer monographs in mathematics, springer, in: Ch. Introduction to the KAM Theory, 2009, pp. 23–58. http://math.bu.edu/people/cew/preprints/introkam.pdf.

[27] J.M. Rogers, A.D. McCulloch, A collocation-Galerkin finite element model of cardiac action potential propagation, Biomed. Eng. IEEE Trans. 41 (8) (1994) 743–757, https://doi.org/10.1109/10.310090.
[28] R. Frank, reportThe Perceptron a Perceiving and Recognizing Automaton, tech. rep., Technical Report 85-460-1.
[29] F. Rosenblatt, The perceptron: a probabilistic model for information storage and organization in the brain, Psychol. Rev. 65 (6) (1958) 386–408, https://doi.org/10.1037/h0042519, arXiv:arXiv:1112.6209, http://doi.apa.org/getdoi.cfm?doi=10.1037/h0042519.
[30] A.B. Novikoff, On Convergence Proofs for Perceptrons, Tech. rep., STANFORD RESEARCH INST MENLO PARK CALIF, 1963.
[31] M. Minsky, S.A. Papert, L. Bottou, Perceptrons: an Introduction to Computational Geometry, MIT press, 2017.
[32] E. Burns, Ecg Library, Mar. 2017. http://lifeinthefastlane.com/ecg-library.

Mario Alan Quiroz Juárez. He received the title of B.S.Electronic Engineer in 2011 from the Instituto Politecnico Nacional (IPN) in the Escuela de Ingenieria Mecanica y Electrica Unidad Culhuacan (ES-IME UC), with a control concentration. He received the degree of Master in Science of Engineering in Microelectronic specialized in analysis, control e implentation of dynamic systems in 2014 at the ESIME UC. He received his Ph.D in the speciality of Communications and Electronics at ESIME UC, IPN. His interest areas are control systems, information security, analysis of biolocal systems and development of hardware for cryptography and medi-cal applications. He is a member of the Association Mexican of Automatic Control (AMCA).

Omar Jiménez Ramírez. He received the title of Communications and Electronic Engineer in 1992 from the Instituto Politécnico Nacional (IPN) at the Escuela de Ingeniería Mecánica y Eléctrica Unidad Zacatenco (ESIME). He received his M.Sc. in Microelectronic in 2003 at the ESIME Unidad Culhuacan (ESIME UC) of the Instituto Polit_ecnico Na-cional, and his Ph.D in the same speciality and school. He is currently teacher and member of the research staff at the IPN. Since 2009 he is in-vited professor at the IPN in the ESIME-UC at the graduate programs of in Microelectronic Engineering. His research interests are control systems with delay, lineal control, analysis of dynamic systems and optimal control. He is a member of the Association Mexican of Automatic Control (AMCA).

José Luis Aragón Vera. He received his M.Sc. in Physics from the Universidad Nacional Autonoma de Mexico (UNAM) in 1988, and his Ph.D. in Materials Physics from the Centro de Investigacion Cientfica y de Educacion Superior de Ensenada, Mexico, in 1990. He is currently Full Professor at the Centre for Applied Physics and Advanced Technology, UNAM. His research projects include several topics from mathematical biology wave propagation in aperiodic structures and Cli_ord algebras.

José Luis Del Río-Correa. He is Doctor from Univer-sidad Aut_onoma Metropolitana (UAM) in 1989. He is currently Professor at Physics Department in UAM. He is a member of the Mexican Physics Society (Mexico). His research interests include statistical physics, complex systems, mathematical physics, thermodynamics, stochastic processes, non-linear phenomena, chaotic systems and fractals.

Rubén Vázquez-Medina. He is an electronics engineer from Universidad Aut_onoma Metropolitana (UAM) in 1989. He received his M.Sc. in Science degree about Electric Communications Engineering in 1993 from the Centro de Investigación y Estudios Avanzados of the Instituto Politécnico Nacional (IPN), and his Ph.D. degree in 2008 from UAM. He is currently Professor at the IPN. From 2006 to 2015 he was an invited teacher at the Security Information Master of the Centro de Estudios Superiores Navales, belonging to the Secretaría de Marina Armada de México. He is a member of the Editorial Board and Reviewer of the IEEE Journal of Latin America. His research interests include dynamical systems, bio{inspired sys-tems, chaotic cryptography, steganography, digital forensics and information security.